COMPARISON OF TM, SIR-B and SIMULATED RADAR IMAGES IN PARTICULAR CONSIDERATION OF FOREST CLASSIFICATION

A. Popella & M. Schardt

DFVLR - WT-DA
8031 Oberpfaffenhofen
Federal Republic of Germany

ISPRS 1988 KYOTO

Abstract:

Digital SAR imagery become more and more subject of scientific data evaluation. At the same there is an increased need for radar image simulators to be used in preparation for future SAR missions. Therefore, the authors initiated an investigation to study the information content of SIR-B data from a well known test-site in comparison to available TM data and, furthermore, to measure the quality of a radar image simulation in the face of real, validated SAR data. Based upon TM data from july 1984, covering a part of the Rhine valley, a detailed classification with respect to tree species and natural age classes of the forested area was performed and verified against available ground truth. More categories such as vineyards, towns etc. were determined by an interactive classification of the TM data in comparison to a topographical map. Two SIR-B data sets from October 1984, covering the same area, however under different geometrical conditions, were also available. Furthermore, there was access to a digital terrain model (DTM) of the common TM/SIR-B kernel area, which means that in conjunction with the TM derived classification the input data sets for a radar image simulation package were available.

Thus a manifold data set was produced and used for an extensive data comparison procedure, especially with respect to a detailed statistical examination. A direct comparison between TM and SIR-B data was made regarding the ability for forest classification. The geometrical influence on radar data was examined. Simulated data and SIR-B data were compared to value the statistical approach within the simulator.

The paper presents in detail the investigation approach as well as the discussion of the results.

1. Introduction

In technology, simulation has been proven to be a well suited aid in helping people to understand (better) complex systems. A Synthetic Aperture Radar (SAR) is an exceeding one, particularly when it is viewed as an end-to-end system.

The final product of a SAR system, the image, must be understood as the result of a complicated processing chain usually consisting of an analog signal generation part on-board (sensor/target interaction) and the digital image generation part on-ground. Its main characteristics depends on the technical specification of the sensor (frequency and polarization) as well as on the actual illumination geometry (grazing angle). Moreover geometrical and radiometrical resolution of the image are dependent upon the adjusted convolution procedure (bandwidth and number of looks to be processed).

Ideally, the technical specification of the sensor and the image generation procedure should fit with the scientific application. For example, the European Remote Sensing satellite (ERS-1), to be launched in 1990, is primarily dedicated to monitor ocean waves, coastal zones and ice. It will operate at C-band with one polarization only (VV) and a mean incidence angle of 23 degrees.

In 1981 the Space Shuttle carried on-board an experimental L-band SAR, the Shuttle Imaging Radar SIR-A. With HH polarization and a fixed incidence angle of about 45 degrees, it was primarily used for geological applications. Ten years later in 1991, the third Shuttle Imaging Radar SIR-C will be launched carrying a three-frequency SAR (L- and C-band provided by the USA, and X-band provided by a bi-lateral German/Italian programme X-SAR) with a multipolarization and multi-incidence-angle capability). Currently are objectives defined and requirements established for an European Advanced Land Applications remote sensing satellite to be launched in the 1990's /1/.

Up until now, it is not clear how to specify an optimal system for various applications. A user has not yet enough experience to transfer his basic interests into properly defined technical specifications. However, the user can reflect on the image data from the interpretation point of view /2/.

Image data can be gained by means of simulation and should be, because the large number of scenes for the various disciplines, areas and alternative technical parameters cannot be acquired by experiments. This would be to expensive as well as extremely time consuming. The optimal specification for a land mission could be specified by simulating the products in advance. Therefore, product simulation should contribute also to the definition of the Advanced Land Application Mission to be performed by an Advance ERS-1 /1/.

Still a big problem is the simulator verification. Several product simulators are available and were investigated in /3/. However, an evaluation of a radar image simulation in the face of real, validated SAR data was not performed up to this study.

In 1987 a manifold data set became available. From an other study, a TM scene from July 1984 covering a part of the Rhine valley as well as a partial classification were available. Two SIR-B scenes from October 1984, covering the same area, however under different geometrical conditions, were also available. By means of a simple geocoding process both SIR-B scenes were adapted to the TM projection. Test areas with well known ground truth data were determined within the TM data set and thus in the SIR-B data too. Therefore, it was possible in a first step to evaluate the real SAR data with the object of getting information about the individual target statistics, as well as the classification ability (forest). Based upon these validated SAR data it was now possible to verify in a second step simulated radar data by a direct comparison with the object of getting a qualitative statement regarding the usefulness of simulated data.

The simulation software package to be investigated is an upgraded version of the Radar Image Simulator of the University of Kansas /4/5/. It requires two input files for processing, a digital terrain model (DTM) and a category data file describing the classes within the data set. The category file was derived from a TM classification, the DTM was provided for the common TM and SIR-B area from the University of Stuttgart, institute for photogrammetry.

In the following chapters the simulation procedure as well as the comparisons between TM and SIR-B data as well as SIR-B and simulated SIR-B data are described.

2. Description of test site

The "Rheingraben" test site was chosen because a detailed TM classification and SIR-B data were available and the test site provides lowland of the lower terrace as well as the mountainous region of the Kaiserstuhl.

The test site is bordered on the north by the "Taubergießen" nature reserve and on the south by the Kaiserstuhl. The entire test site area is located northwest of Freiburg. The regional forest community of the lower terrace is the lowland oak forest. Today the main tree species are oak (quercus robur), white beach (carpinus betulus), birch (betula pendula), maple (acer pseudoplatanus) and linden (tilia platyphyllos).

Along the eastern and western sides of the Rhine the swamp forest occurs. Besides the tree species mentioned above, one also finds poplar, alder (alnus glutinosa), ash (fraxinus excelsior) and different kinds of willows (salix spec.) on the wet habitabs. In the last few decades has douglas fir and pine been planted.

In the mountainous region of the vulcanic Kaiserstuhl, generally beech (fagus sylvatica), oak (quercus petraea) and white beech (carpinus betulus) occurs. A more extended description of the "Rheingraben" test site can be found in /6/.

3. Simulation of radar data

Simulation, as understood in the following, is the process of taking a ground scene which has to be given in a digitized form, and performing the generation of a synthetical radar image by involving the target features, geometrical configurations and technical parameters of the sensor /7/.

The input of the simulation software package is provided by two data files of the same size. One file contains integer numbers describing the actual height of a matrix cell (pixel) above a mean height level, e.g. sea level. The other file equally contains integer numbers which represent the reflectivity category (e.g. trees, vineyards, water ...) of a corresponding pixel of the elevation matrix. The ground location of each pixel is represented in range and azimuth, which is the number of elements in across and along flight direction. In other words, the simulation process depends on an input which can be described as a four-dimensional matrix (range, azimuth, elevation and reflectivity per pixel). The user has to take care for the compatibility of the input reflectivity categories to the backscatter data base, provided by the software.

One of the main features of the simulator is the construction of the so called 'power map'. The power returned to the receiver from each cell in the target scene is calculated independent of all other cells according to the area-extensive form of the radar equation /4/. The scattering coefficient σ^o is computed through a third-order polynominal using the local angle of incidence as the independent variable. The coefficients for the polynominal depend on the measurement frequency and polarization and are stored in the backscatter data base.

Two different ways have been used to construct a synthetical radar image. The first makes use of a simple statistical model. It is assumed that the averaged returned power is related to a multiplicative process involving the expected power and n standard random variables /4/. Thus, the best simulated radar image with high spatial resolution is the "speckled" power map. But it is also possible to take into account system effects. This is done using a power impulse response. It is a filter function where the filter weights are determined through the ratio of desired to given resolution.

Spatial resolution is then modelled by performing a digital convolution of the speckled power map with the image impulse response (rectangular filter window). The final image is then /4/:

$$i(x,y) = \{ r(x,y) \cdot u(x,y) \} * h(x,y)$$

r (x, y) = target reflectivity
u (x, y) = χ^2 random noise (speckle simulation)
h (x, y) = system power impulse response

The advantage of this approach is a minimization of the computer work, but the modelling accuracy is reduced.

The input data sets (DTM and TM derived category file) had 2820 records and 1229 columns. To duplicate the special SIR-B geometry (ascending and descending orbit, left looking antenna), both input files first had to be rotated. For the simulation of the scene 9740, the angle had to be 318,703 degrees which finally gave an image size for the simulation of 2784 columns and 2930 records. The flight altitude was given with 219 km, the mean incidence angle was given with 40.2 degrees. For the scene 4520, the angle was 220,716 degrees which gave an image size for simulation of 2939 records and 2771 columns. Here, the flight altitude was given with 223 km, the mean incidence angle with 50.4 degrees.

For both simulations, the power impulse response function was shaped as a $(\sin x/x)^2$ filter. Four looks were assumed, the resolution was given to be 25 m x 25 m. The L-band was taken with 1500 MHz to be compatible with the stored backscatter data base.

About 840 CPU sec on the big IBM 3090 had to be spent for this simple statistical image simulation. However, the overall computing time including I/O was about 1900 sec. The results are shown in image 3 and 4.

The image simulator was designed to form a SAR image from the power map that the in-phase and quadrature voltages at the output of a linear SAR correlator are independent Gaussian random variables with zero mean and a variance equal to half the received power per pixel.

The intermediate result (the complex voltage map) represents the ideal correlator output with a resolution equal to that of the data base /4/:

$$V(x,y) = \sqrt{\frac{P_r}{2}} \cdot z_1 + j\sqrt{\frac{P_r}{2}} \cdot z_2$$

z_1 and z_2 are independent Gaussian random variables
V (x, y) = complex image
P_r (x, y) = power matrix

The simulation of a nonideal system then requires appropriate processing of the voltage map. The basic idea of this processing route is to perform multilook-averaging for improving the signal-to-noise ratio of the image. Given the complex radar image then the image spectrum can be obtained by means of a discrete Fourier transform. If this image spectrum is subdivided (N subimages, where N is the user defined number of independent looks) and if intensity images are made from the inverse transformed subdivisions, then the resultant images can be added on an intensity basis to produce a radar image of the same scene which has poorer resolution but an improved signal-to-noise ratio /8/. This approach is more realistic but requires a bigger amount of computer time.

Basically the same input data were taken as in the first simulation approach. Only the system transfer function was shaped as a (sin x/x) filter. Due to the Fourier transformation, much more computer time had to be spent. About 5100 CPU sec were needed, the total elapsed time came up to 31800 sec. Within one run, a total of 20 files had to be handled by the software. By virtue of the processing procedure, the already big images were blown up with respect to the FFT routine to the next power of two (zero padding) - a storage capacity of 1.4 Gigabyte was required per run.
The resulting products are shown in image 5 and 6.

4. Geocoding

Both TM scenes from April (18.4.84) and July (7.7.84) were rectified into Gauß-Krüger-Coordinates using the tie-point method, applying a polynomial transformation of second order. The standard deviation was 0.562 pixel in x-and 0.582 pixel in y-direction. The SIR-B images then were adapted to the geocoded TM scene by means of a simple rotation. The rotation angles were calculated by virtue of two pairs of tie-points which were uniquely identificable within the SIR-B as well as in the TM scene.

The TM pixel size (30 m x 30 m) was adapted to the SIR-B pixel size (12.5 m x 12.5 m) before the superposition of the scenes was performed. A visual inspection of both scenes showed a satisfactory position accuracy. The deviation between both scenes were determined to be about one TM pixel.

5. Simulator input

5.1 DTM

The digital terrain model was provided for the study purposes by the institute for photogrammetry of the University of Stuttgart. It was delivered in a Gauß-Krüger-projection with a pixel spacing of 30 m in both directions, the height information given in an integer 4 representation. Some data gaps first had to be filled by an adequate interpolation procedure. Then the complete DTM was two-dimensionally resampled to yield a pixel spacing of 12.5 m correspondingly to the original SIR-B data sampling rate. Then the preprocessed data set was transformed into the integer 2 region and rotated corresponding to the given azimuth angles (138.703 and 220.716 degrees) to allow the simulation of the ascending and descending flight geometry of SIR-B.

5.2 Coverage

The basis of the category file was a multitemporal TM data set of the Rhine valley. TM data and radar data were acquired at different seasons and, therefore, only categories which are only minor subject to phenological change were investigated. Agricultural used areas could not be examined in the simulation because a comparison of simulated radar data which are based on a TM data set of july, to real radar data from october is not allowed due to the great phenological development of such categories within one season. The category file for simulation incorporates the following classes:

- deciduous forest
- coniferous forest
- water (the river Rhine and a few small lakes)
- vine yards
- towns

The forested area was classified appliying the Maximum - Likelihood method to classes of tree species and there natural age classes. The tree classes, mixed deciduous forest, poplar, pine and douglas fir could be seperated with an accuracy of more than 90 % percent. Within the deciduous forest stands it was possible to distinguish three natural age classes of trees with an accuracy of 80 % - 90 % percent /9/. For simulation purposes, a separation into the main classes deciduous and coniferous forest was performed. Water areas were classified by the application of thresholds in the TM channels 4 and 5 (near- and middle infrared). Towns and vineyards could not be separated automatically and were therefore interactively masked on the TM data set and later added to the category file.

6. SIR-B

On October 5, 1984, the second Shuttle Imaging Radar, SIR-B, was launched into orbit aboard the Space Shuttle Challenger. Beside the digital data acquisition capability, SIR-B offered for the first time a multiple-incidence-angle mode enabling investigators to study the relations between radar backscatter and incidence angle through a range of different terrain types and surface covers /10/.

Both SIR-B scenes which have been used for this study were processed by DFVLR itself, each with four looks and a geometrical resolution of about 25 m.

The SIR-B Scene 4520 was taken at the 8th october 1984 during an ascending orbit with the antenna looking to the left. The flight altitude was about 223 km, the mean scene incidence angle was about 50.4 degrees (image 2).

The scene 9740 was taken later during a descending orbit with the antenna again looking to the left. Now the flight altitude was 219 km, the mean incidence angle was about 40.2 degrees (image 1).

In order to reduce the speckle, a simple speckle smoothing algorithm was applied to the original SIR-B dataset. By filtering the data, a reduction of standard deviation can be achieved while preserving a stabil mean value. A detailed description of this algorithm can be found in /11/.

Different filter sizes and noise reduction factors were applied and visually interpreted. Due to this comparison a 7 x 7 sigma filter and a factor of 0.07 was selected for the data investigation.

7. Selection of test areas

In order to verify the simulation and to delineate the information content of SIR-B data according to forest cover classification, test areas were selected for the signature analysis.

Most of the woodland - test areas were taken over from the multitemporal TM-classification mentioned above. The ground truth information was taken from ground truth evaluation, forest maps and forest management plans. In addition to this, four large test areas of deciduous forest were selected due to the classification of the TM data set. With the exception of the mixed deciduous forest, it was not possible to determine all the natural age-classes.

According to the woodland, the following tree classes and their natural age classes were selected:

1. Mixed deciduous forest
   - cultures and thickets (6 test areas)
   - pole timber (3 test areas)
   - timber (9 test areas)
2. Douglas fir.
   - cultures and pole timber (3 test areas)
3. Pine
   - cultures (8 test areas)

For the comparison of woodland and agricultural used areas, in the original SIR-B data three large test areas were selected including different crop types. Within the agricultural used areas no differentiation between different crop types was performed.

Water areas, towns and vineyards were masked interactively on the Thematic-Mapper scene and added to the forest-and agricultural test area later.

With the help of SAS, GINO and PROSA software-packages, available in the DFVLR computer center, the statistical analysis with respect to minimum, maximum, mean, standard deviation, skewness and kurtosis was performed. SAS and GINO also provide graphical displays of grey level histograms and scattergrams. For the digital image processing, the MIDAS system was used.

8. Results

At first, the subsequent signature analysis demonstrates the information content of SIR-B data according to the separation of different tree species and their natural age classes as well as the separation of forested and nonforested areas. Furthermore, the signature of filtered and nonfiltered data is examined. In all classes the mean value and the standard deviation were higher in the scene 9740 (steeper mean incidence angle).
The comparison of TM and SIR-B data is illustrated with a few examples and possibilities of combining these two different data sets will be pointed out.

Secondly, the simulated radar data are compared with the SIR-B data to get a measure of the quality of these data. For the following investigations, only frequency domain simulated data have been used. The simulation results of the simple statistical approach were unacceptable because for all classes, with respect to the real data no similarities in mean, standard deviation and histogram shape could be found.

8.1 Separation of natural age classes within deciduous forest

- SIR-B scene 4520 (mean incidence angle 50.4 degrees)
  A slight trend to a higher reflection of the older trees (timber and old timber) is detected. Same results can be found in /6/, /12/ and /13/. Figure 1 shows the histograms of the unfiltered data of young (cultures and pole timber) and old mixed deciduous forest. Figure 2 shows the histograms of the same classes for the filtered data. The histograms of the filtered data demonstrate a better differentiation of the two classes. For the further comparisons, only histograms of filtered SIR-B were used.

- SIR-B scene 9740 (mean incidence angle 40.2 degrees)
  In spite of a higher standard deviation (21.3 instead of 15.2 for the 4520 scene), a more obvious separation between young and older stands is given (Fig. 3). However, the overlapping range of the histograms is to large for a digital classification and a combination with TM data.

- TM data
  Figure 4 shows in opposite to SIR-B an increase of the grey values which is associated with the decrease of the tree age. Due to the increased shadow portions in the canopy of older stands there is a decreased level of reflection.
  The summer data set was quite sufficient for a reliable separation of the following age classes:

  - cultures and thickets
  - pole timber and high timber
  - low timber and old timber

  A detailed description regarding the general problems of separating age classes can be found in /9/.

8.2 Separation of coniferous and deciduous forest

- SIR-B scene 4520
  The comparison of young pine stands and young stands of mixed deciduous forest illustrates the slight tendency of pine stands to a higher reflection (Fig. 5). Similar results can be found in /14/. However, the histograms of pine cultures and old mixed deciduous forest show a complete overlapping of both signatures (Fig. 6).
  The interesting comparison of old coniferous stands with old mixed deciduous stands could not be performed because no old coniferous stands occur in the investigated test sites. Nevertheless, it is to expect that the old coniferous stands will show also a slightly higher reflection than the old mixed deciduous stands.
  That means that the separation of coniferous and deciduous forest is strongly modified by the age of the trees.

- SIR-B scene 9740
  The histograms of young pine stands and young deciduous forest (Fig. 7) show in spite of a higher standard deviation a stronger differentiation of both classes as in SIR-B scene 4520.

That means that the change of the illumination geometry from 4520 to 9740 orbit allows a better separation for coniferous and deciduous forest, as it was already the case for the separation of natural age classes within deciduous forest.

Again, the comparison of young pine stands and old mixed deciduous stands gives a complete overlapping of both classes (Fig. 8).

- TM data
  With the exception of the classes douglas fir and poplar which could not be separated in the summer data set, a separation of coniferous and deciduous forest was easily performed. More details can be found in /9/.

- Simulated radar data

  - Simulation of scene 9740
    Figure 9 shows the result of the simulation of coniferous and deciduous forest. Compared with Fig. 8, the simulation result is satisfactory for both forest types in that it comes quite close to reality with respect to the values for mean and standard deviation as well as to each histogram shape. However, compared with Fig. 7, the simulation result is not satisfactory because no separation of the classes is performed. Comparing Fig. 7 and 8 it is obvious that the different age of the investigated classes influences the spectral signature of the original SIR-B data. The simulator is provided with a category data base which gives only one set of coefficients per class. Thus, it is not able to distinguish different age classes, as they are given in reality.

  - Simulation of scene 4520
    Figure 10 shows the result of the simulation of coniferous and deciduous forest, now assuming the flight geometry of path 4520. Compared with Fig. 6, the simulation result here is satisfactory for both forest types only in that it gives a correct standard deviation and for each class the right histogram shape. However, the absolute position of the two histograms in Fig. 10 differs significantly from that in Fig. 6.

    This means that the mean difference between the original SIR-B data (about 60 grey values, Fig. 6 and 8) is not simulated. As can be seen in Fig. 9 and 10, the mean difference in the simulated data is about 5 grey values only.
    This example clearly shows that the different geometrical conditions are not correctly represented within the simulated images.

8.3 Separation of douglas fir and pine

- SIR-B 4520
  Compared with pine cultures, douglas fir (thicket and pole timber) shows a slight tendency to a higher reflection within the coniferous forest (Fig. 11). This can be caused either by virtue of different tree species or by the different age of these classes. In order to determine the reason of this, stands of pine and douglas fir of the same age must be compared.

  No statistical examination was performed for the scene 9740 due to the lack of douglas fir test areas.

- TM data
  TM band 4 (near infrared) offered very good possibilities of differentiation between stands of young pine and douglas fir. Douglas fir has a much higher level of reflection than pine in this wavelength (Fig. 12).

8.4 Separation of forested and nonforested areas

In order to investigate the separability of forest from other classes, some different types of non-forested areas were examined.

- Water and forest
  In both SIR-B scenes (4520 and 9740), a separation between water and older decidous forest is possible due to the lower reflection of water (Fig. 13 and 14). The latter one gives a still better differentiation with a neglectable overlapping.

The simulation also provides a clear separation of both classes and a lower reflection of water (Fig. 15 and 16). Opposite to the original SIR-B data, the simulation gives here significant higher mean values for the simulated 4520 scene. Again, it has to be assumed that the different geometrical conditions are not correctly represented within the simulated images.

- Agricultural used areas and forest
  Many different crop types were combined to three large test areas because no ground truth data of the specific area were available. Fig. 17 demonstrates a considerable amount of overlapping, whereas the agricultural area covers the lower grey level range. Again, the scene 9740 provides a better separation of these classes (Fig. 18).

  However, a stratification of forest and nonforest solely by using radar data is not possible due to the still remaining overlapping. Nevertheless, it was found by an additional investigation that SAR data can support the TM data in separating forest and nonforest areas.

- Vineyards and forest
  In the original data sets (4520 and 9740) a great overlapping of both classes as well as a higher reflection of deciduous forest can be seen (Fig. 19 and 20). The simulation gives a quite different result. Opposite to the original data one can find a higher reflection of vineyards and a higher absolute position (Fig. 21 and 22).
  Thus, it can be assumed that the simulator inherent statistic for vineyards does not fit to the reality. Furthermore, the geometrical conditions are not correctly considered within the simulation.

9. Conclusion

It was found that the steeper incidence-angle of scene 9740 improved the separability of the examined classes. Within the forested areas a tendency was found with respect to a differentiation of different tree species and natural age classes. However, the tendency is not strong enough to allow a digital classification of these classes. A minor improvement of the TM derived stratification of forested and nonforested areas was achieved by the additional information of the SIR-B data set.

It was found that radar image simulation might provide a tool for preparing a user community of a future SAR land application satellite. However, to keep pace with the SAR sensor development (multi-polarization/frequency/incidence angle ...), significant simulator improvements must be required. Based on the achieved results it can be stated that the overall geometrical modelling has to be renewed and the backscatter data base has to be upgraded by test-site relevant data. The software structure should be completely reorganized with respect to more powerful computers (array processors) to reduce the tremendous amount of computer time and storage.

References

/1/ ESA: "Remote Sensing for Advanced Land Applications", ESA SP-1075, July 1986

/2/ Hartl Ph., Popella A., Sieber A.,: "SAR Product Simulation", Proc. Workshop on Thematic Applications of SAR Data, Frascati, Italy, 9 - 11 Sept. 1985, ESA SP-257

/3/ INS - University Stuttgart: "SAR Product Simulation", Final Report, ESA Contract: ESTEC No. 6188/85/NL/BI

/4/ Komp E., Frost V., Holtzman J.,: "Reference Manual for the Radar Image Simulator", Technical Report RSL TR 581-2, University of Kansas, January 1983

/5/ Popella A., Wellnitz-Flemming W., Hölzer M., "Erweiterungen des Simulationsprogramms R.I.S. (Radar Image Simulation) der University of Kansas, DFVLR Bericht, November 1984

/6/ Anthony D.A.: "Forest cover analysis using SIR-B data", Proceedings of IGARSS '86 Symposium, 8 - 11 Sept. 1986, Zürich, pp. 1683 - 1687

/7/ Popella A., Sieber A., Hartl Ph., "Simulation of SIR-B Imagery over Freiburg Test-Site", Proc. of IGARSS '84 Symposium, Strasbourg 27 - 30 Aug. 1984, ESA SP-215

/8/ Stiles J. et al.: "Radar Image Analysis and Simulation for the Design of a Geologic mapping Synthetic Aperture Radar: Preliminary Results", Technical Report RSL TR 553-3, University of Kansas, January 1981

/9/ Schardt M.: "Forest classification with TM-Data in the area of Freiburg, Federal Republic of Germany", Proceedings of the Willi Nordberg Symposium, 7 - 9 Sept. 1987, Graz, in print.

/10/ Ford J. et al.: "Shuttle Imaging Radar Views the Earth From Challenger: The SIR-B Experiment", JPL Publication 86-10, March 15, 1986

/11/ Lee J.S.: "A simple speckle smoothing algorithm for Synthetic Aperture Radar images", IEEE Tr. on Systems, Man and Cybernetics, vol. SMC 13, No. 1, January/February 1983, pp. 85 - 89

/12/ Hoffer R.M., Lozano-Garcia D.F., Gillespie D.D., Müller F.W., Ruzed M.J.: "Analysis of multiple incidence angle SIR-B data for determining forest stand characteristics", In: Second Spaceborne Imaging Radar Symposium, JPL, Pasadena, Calif., pp. 159 - 164

/13/ Bönsch E., Winter R., Schreier G.: "Investigations of SAR backscatter for different test areas using two geocoded Seasat SAR scenes", to be published in: IGARSS '88 Symposium, 12 - 16 Sept. 1988, Edinburgh

/14/ Richards J.A., Sun G.Q., Simonett D.S.: "L-Band Radar backscatter modelling of forest stands", IEEE Tr. on GE and RS, vol. GE-25, No. 4, July 1987, pp. 487 - 498

Image 1: Original SIR-B scene 9740

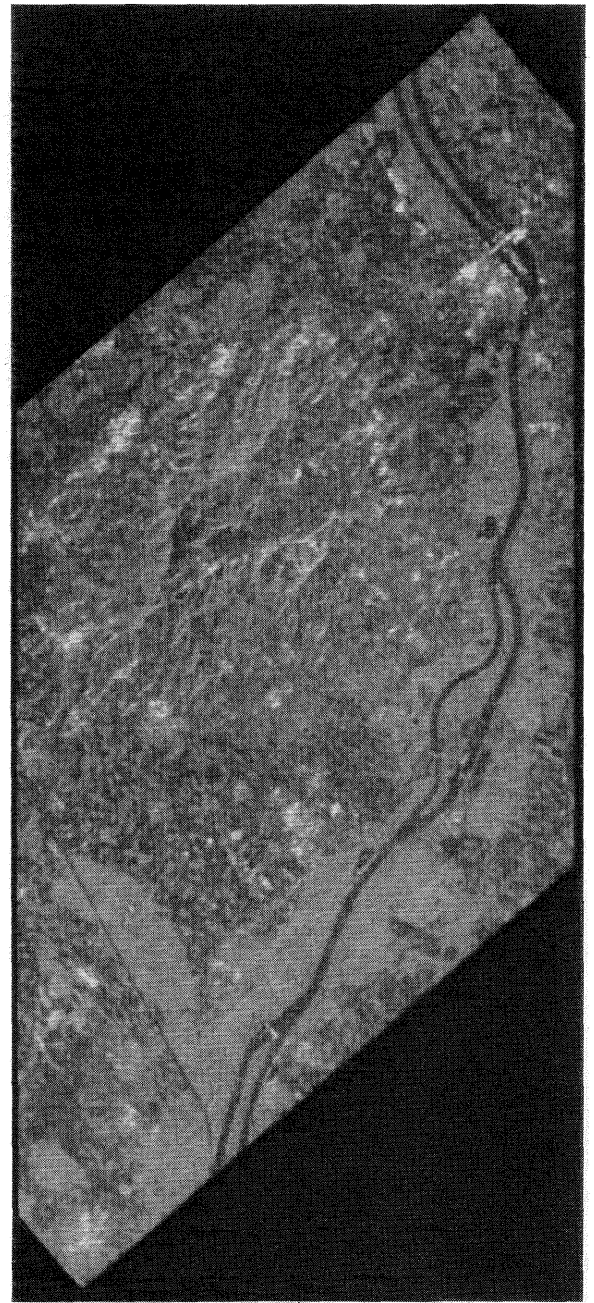

Image 2: Original SIR-B scene 4520

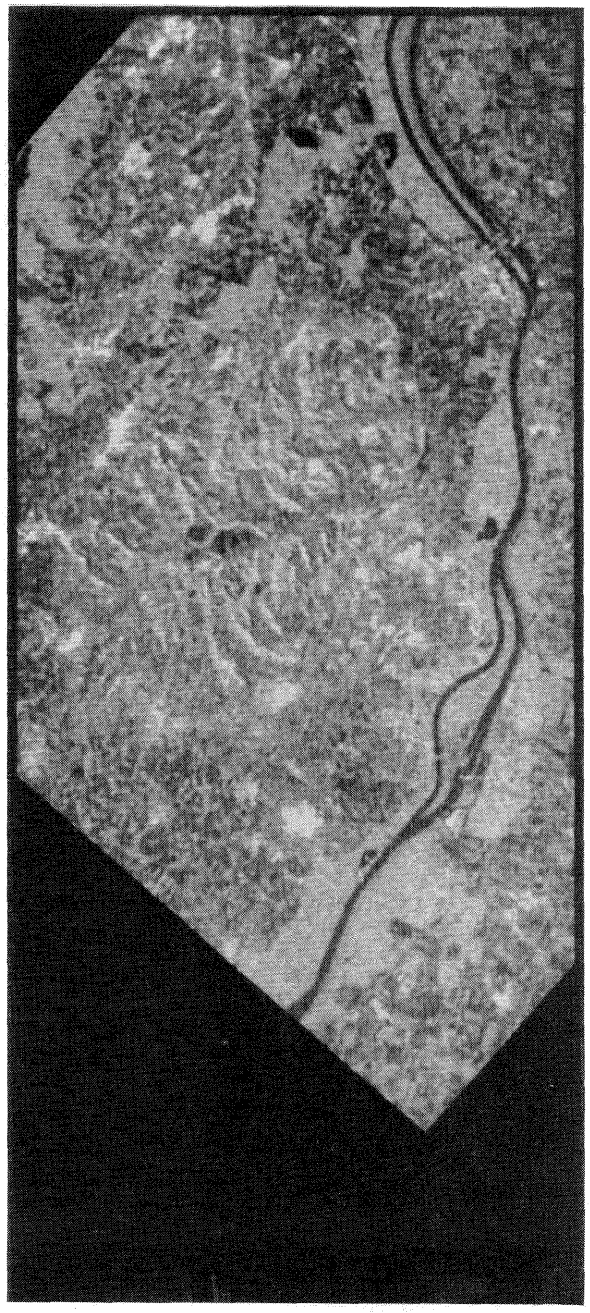

Image 3: Simulated SIR-B scene 9740, spatial filtered

Image 4: Simulated SIR-B scene 4520, spatial filtered

Image 5: Simulated SIR-B scene 9740, frequency filtered

Image 6: Simulated SIR-B scene 4520, frequency filtered

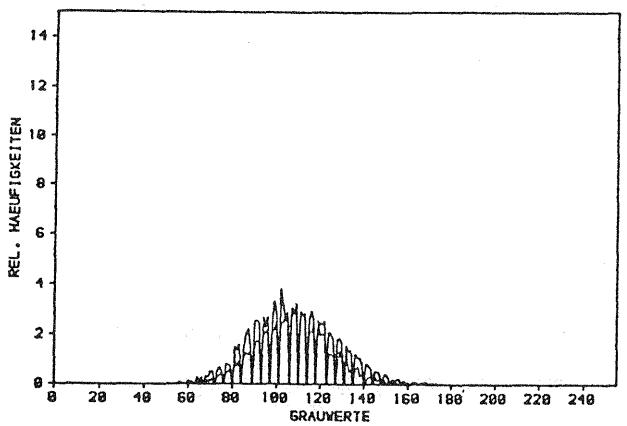

Figure 1: Old and young deciduous forest SIR-B/4520, unfiltered data

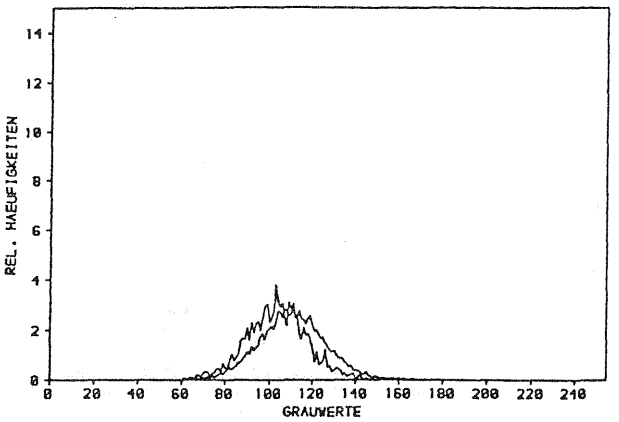

Figure 2: Old and young deciduous forest SIR-B/4520, filtered data

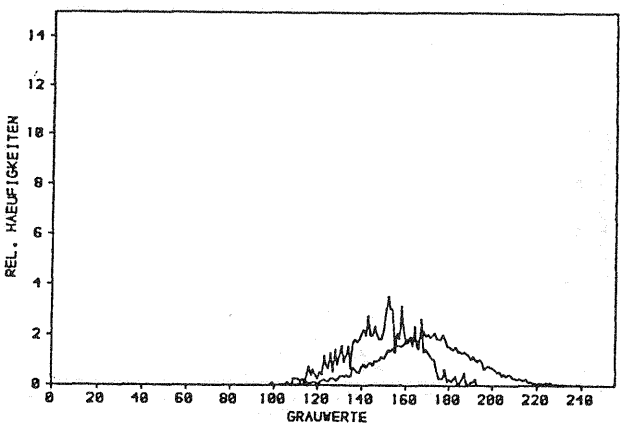

Figure 3: Old and young deciduous forest SIR-B/9740, filtered data

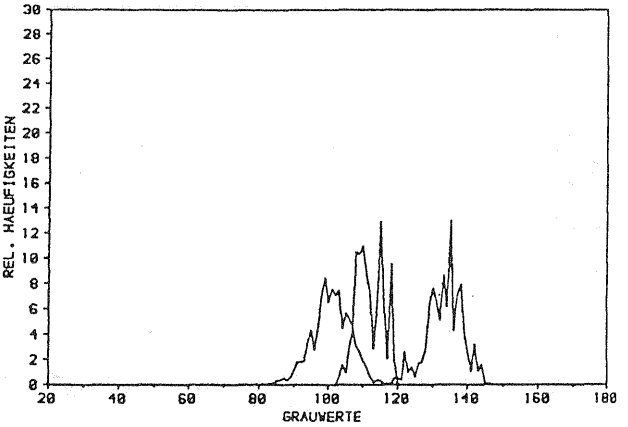

Figure 4: Natural age classes of deciduous forest TM/Band 4

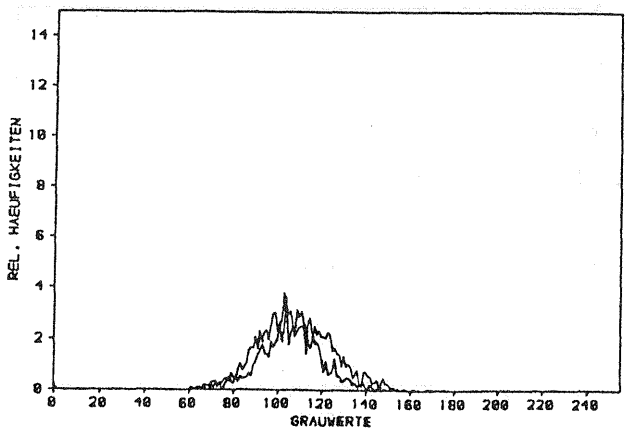

Figure 5: Young deciduous forest and pine SIR-B/4520, filtered data

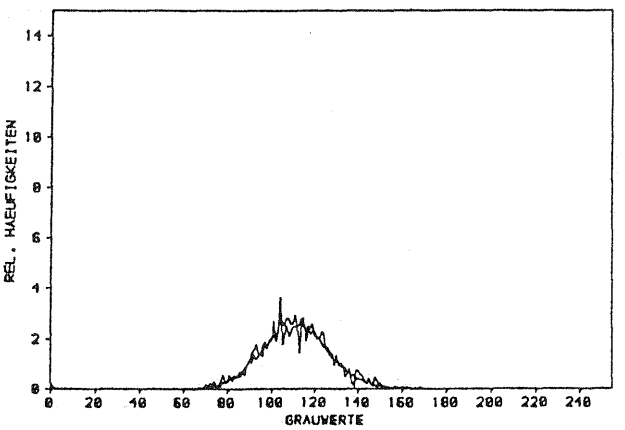

Figure 6: Old deciduous forest and pine SIR-B/4520, filtered data

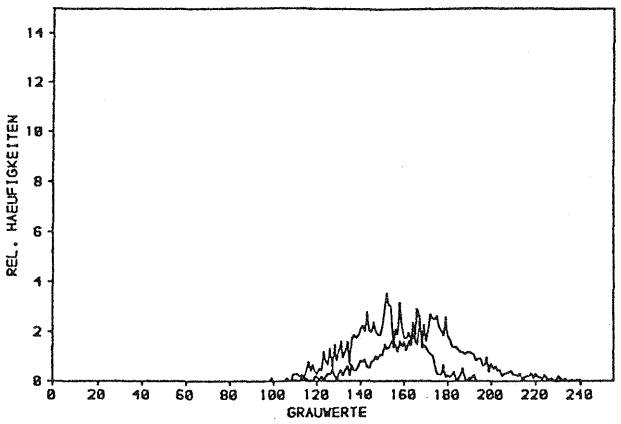

Figure 7: Young deciduous forest and pine SIR-B/9740, filtered data

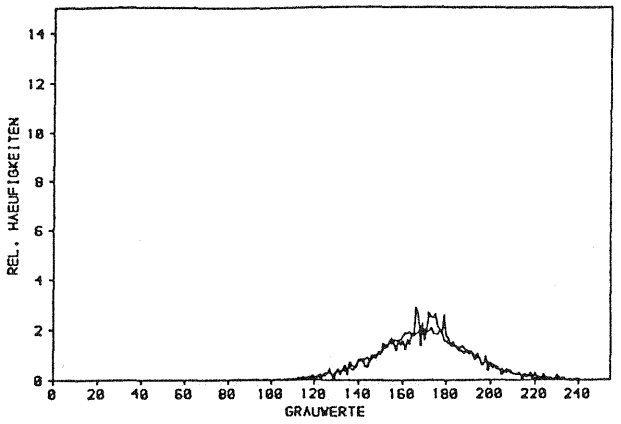

Figure 8: Old deciduous forest and pine SIR-B/9740, filtered data

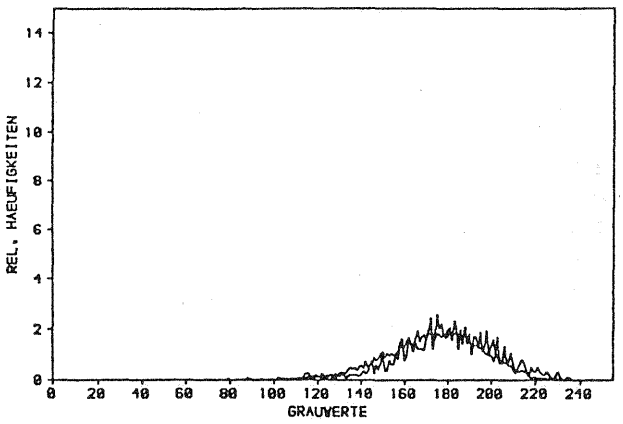

Figure 9: Old deciduous forest and pine simulated data/9740

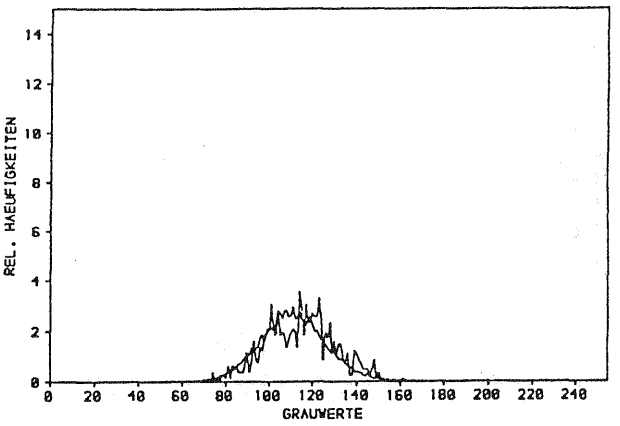

Figure 10: Old deciduous forest and pine simulated data/4520

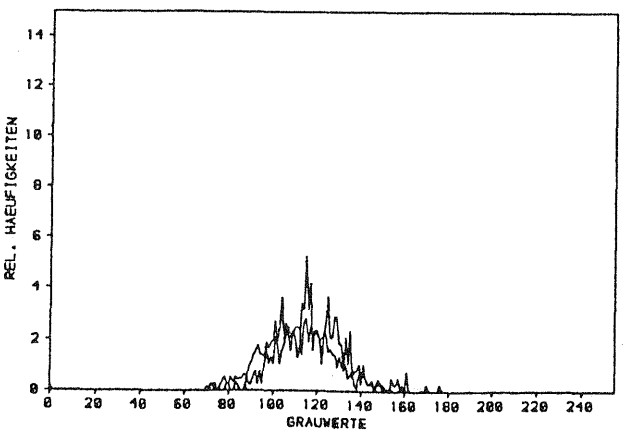

Figure 11: Douglas fir and pine SIR-B/4520, filtered data

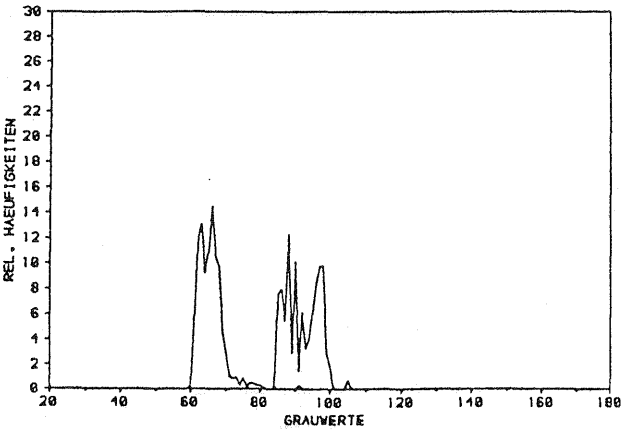

Figure 12: Douglas fir and pine TM/Band 4

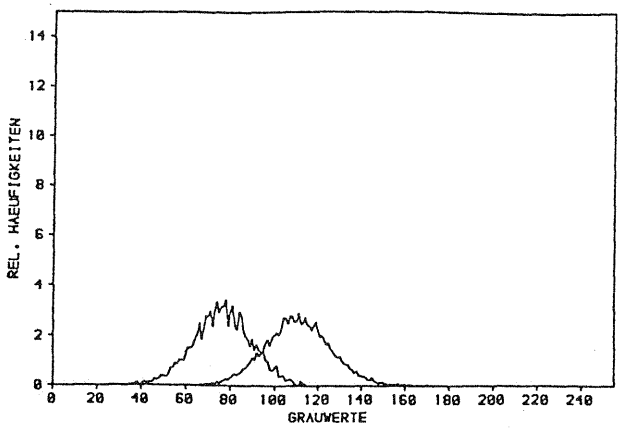

Figure 13: Old deciduous forest and water SIR-B/4520, filtered data

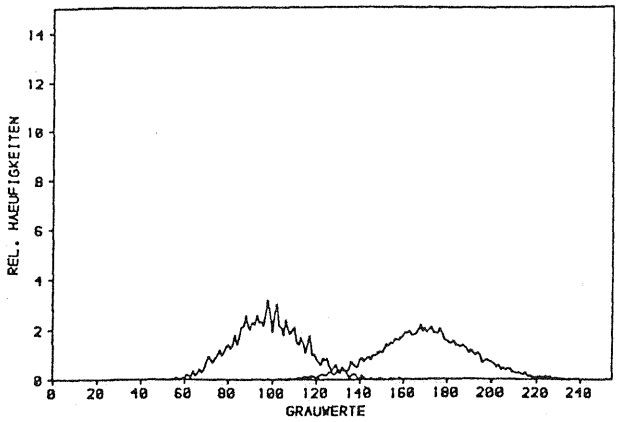

Figure 14: Old deciduous forest and water SIR-B/9740, filtered data

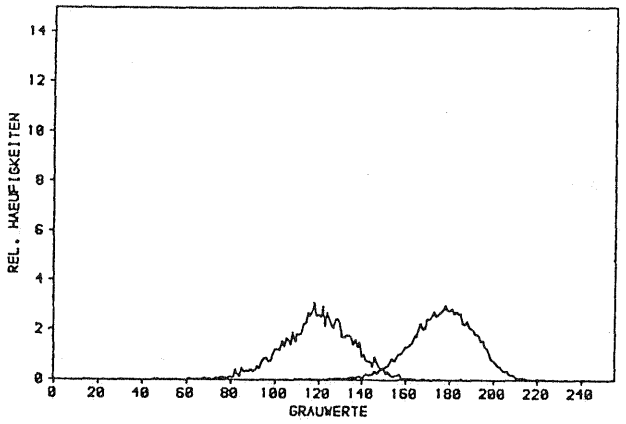

Figure 15: Old deciduous forest and water simulated data/4520

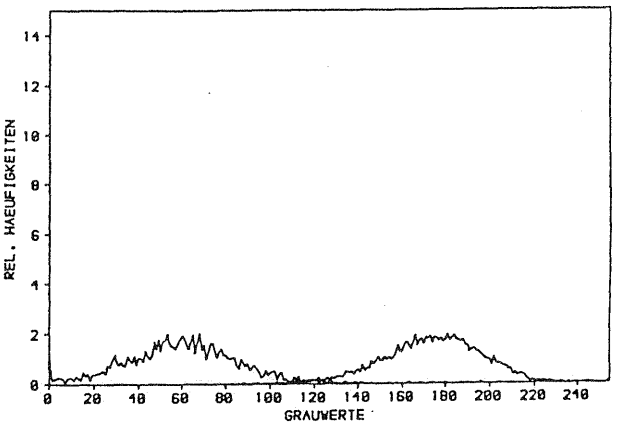

Figure 16: Old deciduous forest and water simulated data/9740

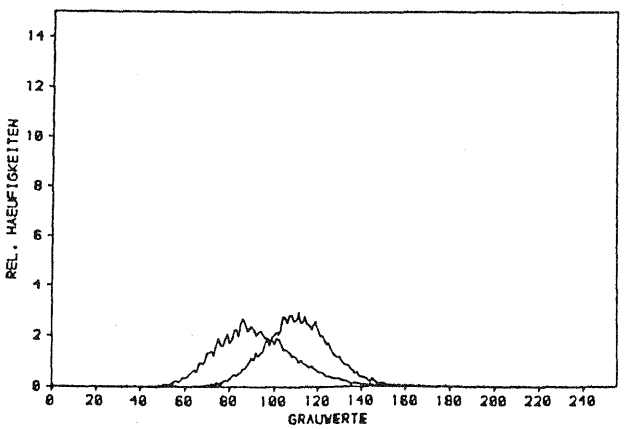

Figure 17: Old deciduous forest and agricultural areas SIR-B/4520, filtered data

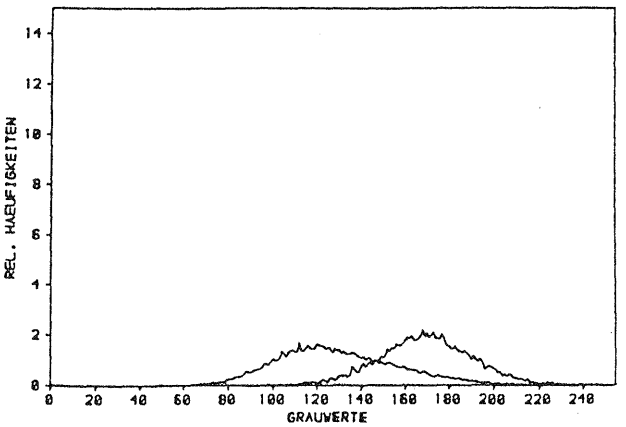

Figure 18: Old deciduous forest and agricultural area SIR-B/9740, filtered data

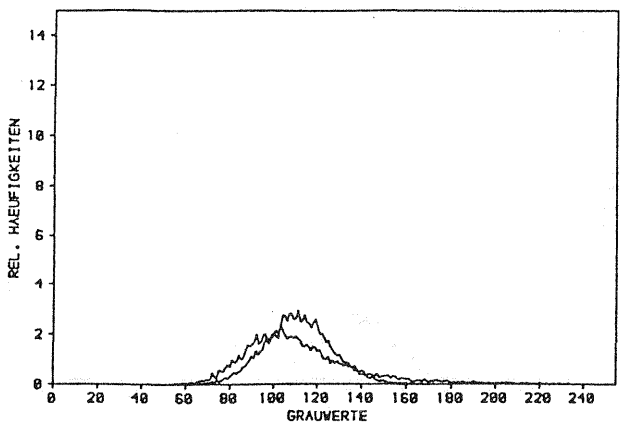

Figure 19: Old deciduous forest and vineyards SIR-B/4520, filtered data

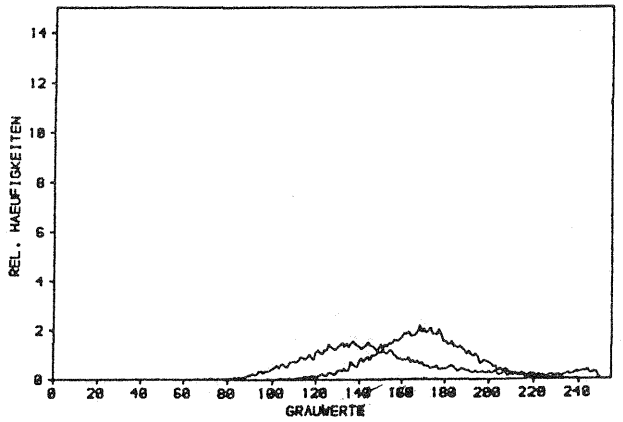

Figure 20: Old deciduous forest and vineyards SIR-B/9740, filtered data

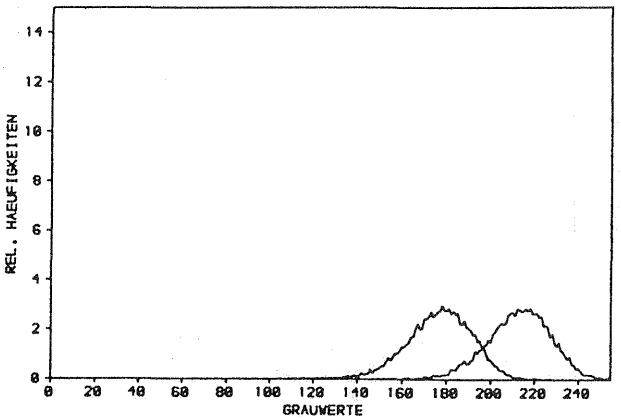

Figure 21: Old deciduous forest and vineyards simulated data/4520

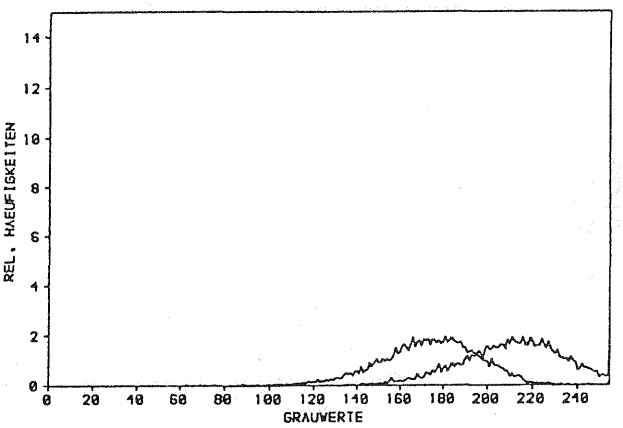

Figure 22: Old deciduous forest and vineyards simulated data/9740